The Journal of Engineering

The 9th International Conference on Power Electronics, Machines and Drives (PEMD 2018)

IET Journals
The Institution of Engineering and Technology

Detection and classification of turn fault and high-resistance connection fault in inverter-fed permanent magnet machines based on high-frequency signals

eISSN 2051-3305
Received on 26th June 2018
Accepted on 30th July 2018
E-First on 13th May 2019
doi: 10.1049/joe.2018.8253
www.ietdl.org

Rongguang Hu[1] ✉, Jiabin Wang[1], Andrew Mills[2], Ellis Chong[3], Zhigang Sun[3]

[1]*Department of Electronics and Electrical Engineering, The University of Sheffield, Sheffield, UK*
[2]*Department of Automatic Control and System Engineering, The University of Sheffield, Sheffield, UK*
[3]*Electrical Capability Group, Rolls-Royce plc, Derby, UK*
✉ *E-mail: rongguanghu@gmail.com*

Abstract: Winding turn fault and high-resistance connection (HRC) fault will lead to different consequences and require different mitigation actions. In this study, the differentiating features between a turn fault and HRC fault are analysed and compared in a three-phase surface-mounted permanent magnet machine fed by the inverter with pulse-width-modulation voltages. The resultant high-frequency components in both voltages and currents are utilised for the fault detection and classification based on the high-frequency impedance and ripple current, without requiring modifications to the machine or interface design. Extensive simulations show that this method is capable of fault detection and classification in both transient and steady-state operations.

1 Introduction

Permanent magnet (PM) machines are being intensively employed in many application areas such as electric vehicle, industrial servo drives, and more-electric aircrafts, due to their excellent features of high efficiency, high torque density etc [1, 2]. Of all the requirements for some typical applications, high reliability is essential. An unexpected fault in PM machine drives may lead to very high repair or replacement cost, or even catastrophic failure. Thus, how to detect and identify potential faults is the key to appropriate mitigating action.

Winding short circuit is the most common form of electrical faults in machines as a result of insulation failure under combined electrical, thermal, and mechanical stress. This failure may lead to inter-turn, phase-to-phase, or phase-to-ground failure [3, 4]. Among these failure modes, an inter-turn fault is the worst fault case since it usually only involves a few turns, resulting in a very low impedance of the short-circuited path. As a result, the large fault current is induced, producing excessive heat which further degrades the insulation between the windings and lamination, and eventually leading to complete failure. However, inter-turn short circuit, also known turn-to-turn short circuit, gives rise to a very benign effect in the motor phase voltage and current. Hence, detection of a single turn short circuit before it develops into catastrophic failure is the most challenging and yet indispensable. Methods of turn fault detection using current signal analysis have been proposed in [5, 6], where specific harmonics are analysed using frequency-based or time-frequency-based, wavelet transform etc techniques. These harmonics are exclusive to certain machines types, reducing its applicability to generic machines. A majority of turn fault (TF) detection methods are based on the phase asymmetry, including the 2nd harmonic in dq currents and voltages [7], negative sequence currents and voltages [8], fundamental component in zero sequence voltages and currents [9] etc. The phase asymmetry resulting from a turn fault is common in most balanced multi-phase machines and, hence, the fault detection process is much more flexible for different applications. However, phase unbalance can be caused by many other factors and is not unique to the turn fault.

Another type of fault, high-resistance connection (HRC) fault, can be caused by a loose connection in any device between the source and the machine or damaged contact surfaces. It can cause local over-heating and subsequently break the connection [10]. Unlike the TF, the damage to the machine caused by HRC is not that severe. In most cases, HRC only deteriorates the operating performance of the machine, such as an increase in torque ripple and reduction in efficiency; thus, it does not necessarily require immediate shutdown. Hence, different faults need to be detected and classified for appropriate remedial action.

Several HRC detection techniques have been proposed in [11–13]. However, the common problems of these detection techniques are that they focus on detecting TFs or HRC faults separately, without the consideration of the other faults. As a matter of fact, similar to the TF, the fundamental feature of an HRC fault is the impedance asymmetry. As a result, many methods proposed originally for the turn fault detection based on the asymmetric features will lead to similar results for the HRC fault. Thus, further analysis is needed.

The detection and classification of TF and HRC based on zero sequence voltage and negative sequence current in an induction machine is proposed in [14]. Both amplitude and phase angle of three-phase currents are obtained and compared to find a different pattern for the two fault types. In [15], the phase angle of both fundamental current and impedance are used to realise the fault classification. However, the impedance phase angle obtained by the prior measured machine parameters may change under different operating conditions. In addition, the technique is only valid in steady-state conditions and will lead to a false alarm in transient.

The feature of differences in the phase impedances caused by turn fault and HRC fault in high-frequency region is more significant when the inductive effect is much more dominant than the resistive effect, making it possible to distinguish them. Therefore, a new method based on the high-frequency impedance and PWM ripple current is proposed in this paper, aimed to detect and classify the turn fault and HRC fault.

2 Fault analysis

2.1 Turn fault conditions

A turn fault is caused by insulation breakdown between turns in the same phase winding. The resistance of the insulation can decrease from a few MΩ to a very small value, and reach 0 in the most serious situation, creating a short circuit loop. Without loss of generality, the equivalent circuit model of three-phase surface-

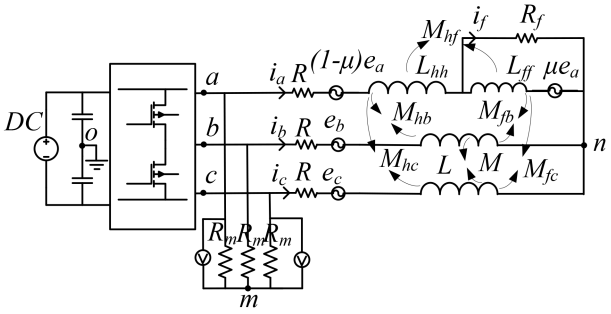

Fig. 1 *Equivalent circuit and parameters with turn fault*

mounted permanent magnet (SPM) assuming turn fault occurs in phase A, with the conventional inverter drive system, is illustrated in Fig. 1. The windings of phase A is divided into two parts, the healthy part (*h*), and the faulted part (*f*) with an additional short circuit resistor. The percentage of the number of the shorted turns over the total number of the turns in phase A is denoted as μ. The self-inductances in the healthy and faulted parts, their mutual inductances, and the mutual inductances between phase A and the other phases are also defined. As the back-EMF is almost linearly proportional to the number of turns, the EMFs in both healthy and faulted parts can be expressed as functions of μ. Based on the circuit, the model under the fault conditions can be expressed in (1). The self-inductance and mutual inductance can be obtained from finite element analysis [16].

$$\boldsymbol{U}_s^{\mathrm{TF}} = \boldsymbol{R}_s^{\mathrm{TF}}\boldsymbol{i}_s^{\mathrm{TF}} + \boldsymbol{L}_s^{\mathrm{TF}}\mathrm{d}\boldsymbol{i}_s^{\mathrm{TF}}/\mathrm{d}t + \boldsymbol{e}_s^{\mathrm{TF}} \tag{1}$$

where $\boldsymbol{U}_s^{\mathrm{TF}} = [u_{ah}\, u_{af}\, u_{bn}\, u_{cn}]^{\mathrm{T}}, \boldsymbol{i}_s^{\mathrm{TF}} = [i_a\ i_b\ i_c\ i_f]^{\mathrm{T}}$

$$\boldsymbol{e}_s^{\mathrm{TF}} = \begin{bmatrix} 1-\mu & & & \\ & \mu & & \\ & & 1 & \\ & & & 1 \end{bmatrix}, \boldsymbol{R}_s^{\mathrm{TF}} = R\begin{bmatrix} 1-\mu & & & \\ & \mu & & \\ & & 1 & \\ & & & 1 \end{bmatrix}$$

$$\boldsymbol{L}_s^{\mathrm{TF}} = \begin{bmatrix} L_{hh} & M_{hf} & M_{hb} & M_{hc} \\ M_{hf} & L_{ff} & M_{fb} & M_{fc} \\ M_{hb} & M_{fb} & L & M \\ M_{hc} & M_{fc} & M & L \end{bmatrix}$$

u_{bn} and u_{cn} are the phase voltages for phases B and C. u_{ah} and u_{af} are the voltages in the healthy and faulted parts of phase A, whose sum is the phase voltage of phase A. The voltage across the faulted turns, u_{af}, can also be calculated by the product of the fault current, i_f, and the short circuit resistance, shown in (2). The short circuit resistance R_f is assumed zero for the sake of simplicity. Then $u_{af} = 0$, and $u_{an} = u_{ah}$.

$$\begin{aligned} u_{af} &= R_f i_f \\ u_{an} &= u_{ah} + u_{af} \end{aligned} \tag{2}$$

In fault conditions, the following approximations may be considered for the further simplification:

$$\begin{cases} M \simeq M_{hb} + M_{fb} \simeq M_{hc} + M_{fc} \\ L \simeq L_{hh} + 2M_{hf} + L_{ff} \end{cases} \tag{3}$$

In most cases, the neutral point, *n*, of the three-phase windings is floating (not connected to ground) and also inaccessible, as shown in Fig. 1. Thus, the phase voltage referred to *n* cannot be measured directly. The difference between the phase voltages u_{an}, u_{bn}, u_{cn} and the inverter output voltages u_{ao} u_{bo}, u_{co}, referred to the DC link midpoint, is the zero sequence voltage u_{no}, which neither can be measured. Thus, in order to build the relationship between the measured voltages and the phase currents, u_{no} needs to be eliminated. By employing a three-phase resistor network to form an artificial neutral point *m*, shown in Fig. 1, the phase voltages referred to point *m* can be expressed in (4), where u_{no} is eliminated naturally. These voltages are measured and used to examine the relationship with phase currents

$$\begin{cases} u_{am} = u_{ao} - \dfrac{u_{ao}+u_{bo}+u_{co}}{3} = u_{an} - \dfrac{u_{an}+u_{bn}+u_{cn}}{3} \\ u_{bm} = u_{bo} - \dfrac{u_{ao}+u_{bo}+u_{co}}{3} = u_{bn} - \dfrac{u_{an}+u_{bn}+u_{cn}}{3} \\ u_{cm} = u_{co} - \dfrac{u_{ao}+u_{bo}+u_{co}}{3} = u_{cn} - \dfrac{u_{an}+u_{bn}+u_{cn}}{3} \end{cases} \tag{4}$$

Accordingly, voltage equations are modified, and the expression of the measured voltages is shown in (5)

$$\boldsymbol{U}_m^{\mathrm{TF}} = \boldsymbol{R}_{sm}^{\mathrm{TF}}\boldsymbol{i}_s^{\mathrm{TF}} + \boldsymbol{L}_{sm}^{\mathrm{TF}}\mathrm{d}\boldsymbol{i}_s^{\mathrm{TF}}/\mathrm{d}t + \boldsymbol{e}_m^{\mathrm{TF}} \tag{5}$$

where

$$\boldsymbol{U}_m^{\mathrm{TF}} = [u_{am}\ u_{bm}\ u_{cm}]^T, \boldsymbol{e}_m^{\mathrm{TF}} = [e_a - \bar{e}\ e_b - \bar{e}\ e_c - \bar{e}]^{\mathrm{T}},$$
$$\bar{e} = \frac{e_a + e_b + e_c}{3}$$

$$\boldsymbol{L}_{sm}^{\mathrm{TF}} = \begin{bmatrix} L & M & M & -\frac{2}{3}(M_{hf}+L_{ff}) + \frac{1}{3}(M_{fb}+M_{fc}) \\ M & L & M & \frac{1}{3}(M_{hf}+L_{ff}) - \frac{2}{3}M_{fb} + \frac{1}{3}M_{fc} \\ M & M & L & \frac{1}{3}(M_{hf}+L_{ff}) + \frac{1}{3}M_{fb} - \frac{2}{3}M_{fc} \end{bmatrix},$$

$$\boldsymbol{R}_{sm}^{\mathrm{TF}} = \begin{bmatrix} R & 0 & 0 & -\frac{2}{3}\mu R \\ 0 & R & 0 & \frac{1}{3}\mu R \\ 0 & 0 & R & \frac{1}{3}\mu R \end{bmatrix}$$

As the voltages are generated in the form of PWM, they contain rich high-frequency harmonics. Thus, the high-frequency components of voltages and currents can also be evaluated by neglecting the back-EMFs because they are at a much lower frequency. Also, as the switching frequency is set at 10 kHz, and with the consideration of the spectrum of measured voltages u_{am}, shown in Fig. 2, the high-frequency components around 20 k Hz are adopted and obtained by bandpass filters, according to [17]. At such frequency, the effect of resistance can be ignored due to the dominance of inductance. Thus, unified voltage equations at high frequency can be derived and written in (6), where the subscript 'HF' in voltages and currents denotes their high-frequency components and *s* denotes the Laplace operator

$$\boldsymbol{U}_{m\_\mathrm{HF}}^{\mathrm{TF}} = \boldsymbol{R}_{sm}^{\mathrm{TF}}\mathrm{d}\boldsymbol{i}_{s\_\mathrm{HF}}^{\mathrm{TF}}/\mathrm{d}t = s\boldsymbol{L}_{sm}^{\mathrm{TF}}\boldsymbol{i}_{s\_\mathrm{HF}}^{\mathrm{TF}} \tag{6}$$

where

$$\boldsymbol{U}_{m\_\mathrm{HF}}^{\mathrm{TF}} = [u_{am\_\mathrm{HF}}\ u_{bm\_\mathrm{HF}}\ u_{cm\_\mathrm{HF}}\ ]^{\mathrm{T}},$$
$$\boldsymbol{i}_{s\_\mathrm{HF}}^{\mathrm{TF}} = [i_{a\_\mathrm{HF}}\ i_{b\_\mathrm{HF}}\ i_{c\_\mathrm{HF}}\ i_{f\_\mathrm{HF}}]^{\mathrm{T}}$$

The high-frequency short circuit current due to the turn fault can be predicted using (7), and the relationship between the three-phase high-frequency currents and voltages is characterised by the complex operational impedance matrix $s\boldsymbol{L}_m^{\mathrm{TF}}$ in (8)

$$\begin{aligned} i_{f\_\mathrm{HF}} &= (L_{ff}+M_{hf})i_{a\_\mathrm{HF}} + M_{fb}i_{b\_\mathrm{HF}} + M_{fc}i_{c\_\mathrm{HF}} \\ &= (L_{ff}+M_{hf}-M_{fc})i_{a\_\mathrm{HF}} + (M_{fb}-M_{fc})i_{b\_\mathrm{HF}} \end{aligned} \tag{7}$$

$$\boldsymbol{U}_{m\_\mathrm{HF}}^{\mathrm{TF}} = s\boldsymbol{L}_m^{\mathrm{TF}}\boldsymbol{i}_{m\_\mathrm{HF}}^{\mathrm{TF}} \tag{8}$$

where $\boldsymbol{i}_{m\_\mathrm{HF}}^{\mathrm{TF}} = [i_{a\_\mathrm{HF}}\ i_{b\_\mathrm{HF}}\ i_{c\_\mathrm{HF}}]^{\mathrm{T}}$

$$\boldsymbol{L}_m^{\mathrm{TF}} = \begin{bmatrix} L + A(L_{ff} + M_{hf}) & M + AM_{fb} & M + AM_{fb} \\ M + B(L_{ff} + M_{hf}) & L + BM_{fb} & M + BM_{fc} \\ M + C(L_{ff} + M_{hf}) & M + CM_{fb} & L + CM_{fc} \end{bmatrix}$$

$$A = -\frac{-2(M_{hf} + L_{ff}) + M_{fb} + M_{fc})}{3L_{ff}}$$

$$B = \frac{(M_{hf} + L_{ff}) - 2M_{fb} + M_{fc}}{3L_{ff}}$$

$$C = \frac{(M_{hf} + L_{ff}) - M_{fb} - 2M_{fc}}{3L_{ff}}$$

2.2 High-resistance fault conditions

When a HRC fault occurs, the machine windings can be modelled with an additional resistor ΔR connected to the faulted phase winding, as shown in Fig. 3, assuming that the fault occurs in phase A. The phase voltage equations in the HRC condition can be expressed as (9)

$$\boldsymbol{U}_s^{\mathrm{HRC}} = \boldsymbol{R}_s^{\mathrm{HRC}}\boldsymbol{i}_m^{\mathrm{HRC}} + \boldsymbol{L}_s^{\mathrm{HRC}}\mathrm{d}\boldsymbol{i}_m^{\mathrm{HRC}}/\mathrm{d}t + \boldsymbol{e}_s^{\mathrm{HRC}} \tag{9}$$

where

$$\boldsymbol{U}_s^{\mathrm{HRC}} = [u_{am}\ u_{bm}\ u_{cm}]^T, \boldsymbol{i}_m^{\mathrm{HRC}} = [i_a\ i_b\ i_c\ ]^T,$$
$$\boldsymbol{e}_s^{\mathrm{HRC}} = [e_a\ e_b\ e_c]^T$$

$$\boldsymbol{L}_s^{\mathrm{HRC}} = \begin{bmatrix} L & M & M \\ M & L & M \\ M & M & L \end{bmatrix}, \boldsymbol{R}_s^{\mathrm{HRC}} = \begin{bmatrix} R + \Delta R & 0 & 0 \\ 0 & R & 0 \\ 0 & 0 & R \end{bmatrix}$$

With the same consideration and the same circuit configuration of the additional resistor network to generate the artificial neutral point m shown in Fig. 3, the expression of the measured phase voltages against m is shown in (10)

$$\boldsymbol{U}_m^{HRC} = \boldsymbol{R}_m^{HRC}\boldsymbol{i}_m^{HRC} + \boldsymbol{L}_m^{HRC}\mathrm{d}\boldsymbol{i}_m^{HRC}/\mathrm{d}t + \boldsymbol{e}_m^{HRC} \tag{10}$$

where

$$\boldsymbol{U}_m^{\mathrm{HRC}} = [u_{am}\ u_{bm}\ u_{cm}]^{\mathrm{T}}, \boldsymbol{e}_m^{\mathrm{HRC}} = [e_a - \bar{e}\ e_b - \bar{e}\ e_c - \bar{e}]^{\mathrm{T}},$$

$$\boldsymbol{R}_m^{\mathrm{HRC}} = \begin{bmatrix} R + \frac{2}{3}\Delta R & 0 & 0 \\ 0 & R - \frac{1}{3}\Delta R & 0 \\ 0 & 0 & R - \frac{1}{3}\Delta R \end{bmatrix},$$

$$\boldsymbol{L}_m^{\mathrm{HRC}} = \begin{bmatrix} L - M & 0 & 0 \\ 0 & L - M & 0 \\ 0 & 0 & L - M \end{bmatrix} = (L - M)\begin{bmatrix} 1 & 0 & 0 \\ 0 & 1 & 0 \\ 0 & 0 & 1 \end{bmatrix}$$

After the simplification and neglect of back-EMF and resistive impedance at high frequency, the relationship between the high-frequency voltages and high-frequency currents is expressed in (11)

$$\boldsymbol{U}_{m\_\mathrm{HF}}^{\mathrm{HRC}} = \boldsymbol{L}_m^{\mathrm{HRC}}\mathrm{d}\boldsymbol{i}_{m\_\mathrm{HF}}^{\mathrm{HRC}}/\mathrm{d}t = s\boldsymbol{L}_m^{\mathrm{HRC}}\boldsymbol{i}_{m\_\mathrm{HF}}^{\mathrm{HRC}} \tag{11}$$

where

$$\boldsymbol{U}_{m\_\mathrm{HF}}^{\mathrm{HRC}} = [u_{am\_\mathrm{HF}}\ u_{bm\_\mathrm{HF}}\ u_{cm\_\mathrm{HF}}]^{\mathrm{T}}, \boldsymbol{i}_{m\_\mathrm{HF}}^{\mathrm{HRC}} = [i_{a\_\mathrm{HF}}\ i_{b\_\mathrm{HF}}\ i_{c\_\mathrm{HF}}]^{\mathrm{T}}$$

3 Fault detection and classification

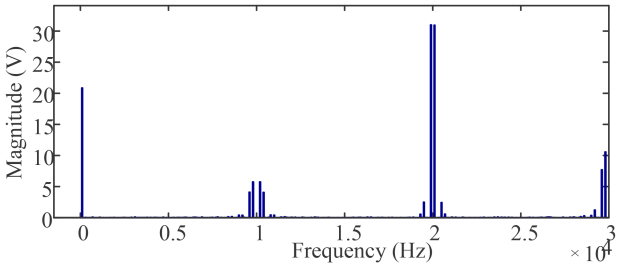

Fig. 2 *Spectrum of the voltage u_{am}*

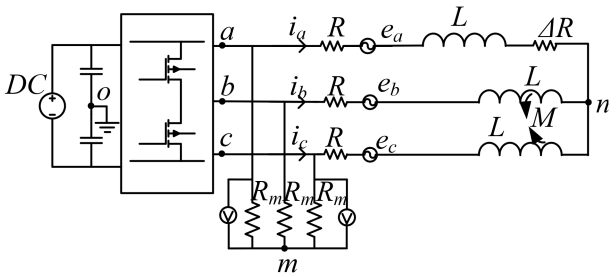

Fig. 3 *Equivalent circuit and parameters with high-resistance connection fault*

Comparing the high-frequency voltage as in (8) and (10), it is apparent that the difference lies in the inductance matrix. For the HRC fault condition, the inductance matrix is identical to that in healthy conditions, being symmetrical and characterised by the synchronous inductance. This implies that the relationships between high-frequency voltages and the corresponding high-frequency currents are identical for three phases in terms of phase shift and magnitude ratio, regardless of whether the voltages are symmetrical or not. For the convenience of data processing, the ratio of the RMS values of the high-frequency voltage and high-frequency current, i.e. the high-frequency impedance, is calculated to represent their relationship, shown in (12), where x, y denotes a, b, and c, and rms denotes the RMS value. From the analysis, the three-phase high-frequency impedances should remain equal in the HRC fault condition as they are in healthy condition, shown in (13). However, as the symmetry at the fundamental frequency is broken due to the HRC fault, the voltage modulation indexes are different among the three phases. As the spectrum of the output PWM voltages are dependent on the modulation index, both the high-frequency voltages and currents are no longer identical in the three phases

$$Z_{x\_\mathrm{HF}} = \frac{u_{x-\mathrm{HF}}^{\mathrm{rms}}}{i_{x-\mathrm{HF}}^{\mathrm{rms}}} \tag{12}$$

$$Z_{x\_\mathrm{HF}} = Z_{y\_\mathrm{HF}} \tag{13}$$

For turn fault conditions, the inductance matrix shown in (8) does not have the same characteristic. With the parameters obtained from finite element analysis, the relationship between the high-frequency voltages and currents can be evaluated. Unlike the HRC fault conditions, the high-frequency impedances in each phase calculated in the turn fault conditions are unequal to each other. Thus, a turn fault introduces asymmetry into both the fundamental and high-frequency components. Consequently, apart from the high-frequency impedance, the high-frequency voltages and currents also deviate from each other among the three phases due to the asymmetrical modulation indexes.

Based on the foregoing analysis, the features of modulation indexes, high-frequency voltages, high-frequency currents, and high-frequency impedances among the three phases are shown in Table 1.

From Table 1, it is evident that by applying the features of high-frequency currents, a turn fault or HRC fault can be detected but cannot be distinguished. By applying the features of the high-frequency impedance, these two types of fault can be classified. To

Table 1 Features comparison in healthy and fault conditions

Healthy condition	High-resistance fault	Turn fault
symmetrical modulation index	asymmetrical modulation index	asymmetrical modulation index
$u_{x\_HF}^{rms} = u_{y\_HF}^{rms}$	$u_{x\_HF}^{rms} \neq u_{y\_HF}^{rms}$	$u_{x\_HF}^{rms} \neq u_{y\_HF}^{rms}$
$i_{x\_HF}^{rms} = i_{y\_HF}^{rms}$	$i_{x\_HF}^{rms} \neq i_{y\_HF}^{rms}$	$i_{x\_HF}^{rms} \neq i_{y\_HF}^{rms}$
$Z_{x\_HF} = Z_{y\_HF}$	$Z_{x\_HF} = Z_{y\_HF}$	$Z_{x\_HF} \neq Z_{y\_HF}$

Table 2 Ratios of RMS currents and high frequency impedance in healthy and fault conditions

Healthy condition	High-resistance fault	Turn fault
$k_{i\_xy} = 1$	$k_{i\_xy} \neq 1$	$k_{i\_xy} \neq 1$
$k_{Z\_xy} = 1$	$k_{Z\_xy} = 1$	$k_{Z\_xy} \neq 1$

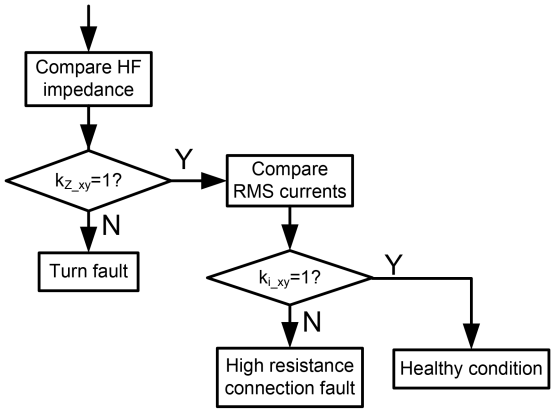

Fig. 4 *Faults detection and classification steps*

Table 3 Design and operational parameters

Machine topology: surface-mounted, fractional slot per pole	
number of pole pairs	7
number of slots	12
axial length (active), mm	118
outer diameter (excluding case), mm	150
number of turns per coil	8
number of coils per phase	4
maximum/base speeds, r/min	5000/1350
peak/continuous torques, N m	70/35
torque constant, N m/A peak	0.415
efficiency at 1350 rpm/33.5 N m	94.4
continuous current, A peak/rms	85/60.5
maximum current, A peak/rms	170/121
phase resistance at 120°C, mΩ	20.8
synchronous inductance, mH	0.344
flux linkage per phase, mWb	39.6
back-EMF constant, V peak s/rad	0.277

avoid dependency on the machine parameters and operating conditions, the fault indicators are defined as the ratios of the selected variables between two phases, shown in (14) and (15). Based on Table 1, the features of the ratios in the health and two different fault conditions are shown in Table 2. By examining the ratios, these two types of faults can be detected and classified with the flow chart shown in Fig. 4. As a turn fault needs to be detected more swiftly to avoid significant damage and the deviation of impedance ratio from 1 is evaluated first. If it is unequal to 1, then the turn fault can be diagnosed immediately. If not, then check the ratios of RMS high-frequency currents to determine whether the machine is healthy or an HRC fault has occurred

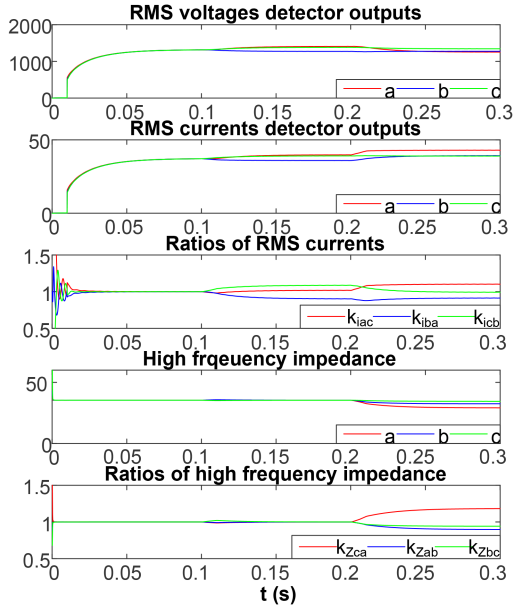

Fig. 5 *Responses of high-frequency currents ratios and high-frequency impedance ratios in healthy, HRC fault, and turn fault conditions*

$$k_{i\_xy} = \frac{i_{x-HF}^{rms}}{i_{y-HF}^{rms}}, x \neq y \tag{14}$$

$$k_{Z\_xy} = \frac{Z_{x\_HF}}{Z_{y\_HF}} \tag{15}$$

4 Simulation results

The machine under study is a three-phase SPM machine with 12 slots and 7 pole pairs. The main design and operational parameters are shown in Table 3. The machine is controlled by an outer speed loop and two inner current loops in the dq reference frame. One turn short-circuit fault is injected in phase A to represent the turn fault conditions, and 0.1 Ω extra resistor is added to the winding of phase A to represent the HRC fault conditions.

Fig. 5 shows the detection result of the RMS currents ratios and high-frequency impedance ratios in healthy, HRC fault, and turn fault conditions. The machine operates at 1000 r/min with a load of 150 A current initially. At 0.1 s, 0.1 Ω additional resistance is activated in phase A to simulate the HRC fault caused by poor contact. This fault is removed at 0.2 s when one turn fault in phase B is injected and lasted until 0.3 s. It should be noted that the detector outputs represents the processed signals proportional to the RMS voltage and current, and the initial deviations of the current and impedance ratios from 1.0 are caused by the delay in the RMS computation.

It is evident that during the healthy state, the RMS high-frequency currents in the three phases are almost identical, so are the high-frequency impedances. Hence, both the ratios between two adjacent phases are 1. When an HRC fault occurs, the RMS currents are different from each other, leading to the ratios unequal to 1. However, the impedance ratios are hardly affected, remaining close to the reference value of 1.0. When a turn fault occurs, both the ratios of the RMS currents and the high-frequency impedances deviate from 1.0. Thus, it is convenient to detect and classify the two faults based on the two ratios.

The effects of the transient state on the ratios are also examined by simulation. In this case, the machine operates initially at 500 r/min with the current of 100 A. At 0.1 s, a step change of current from 100 to 150 A takes place, followed by an increase in speed from 500 to 1500 r/min between 0.2 and 0.5 s, as shown in Fig. 6. The HRC fault is activated from 0.3 to 0.4 s, whereas the turn fault is activated from 0.4 to 0.5 s. The detection results are shown in Fig. 7. It can be seen that the ratios of the high-frequency current and impedance are not affected by the current step change or speed

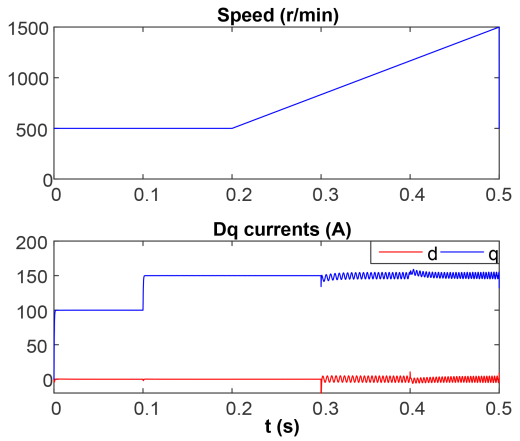

Fig. 6 *Transient states in the simulation*

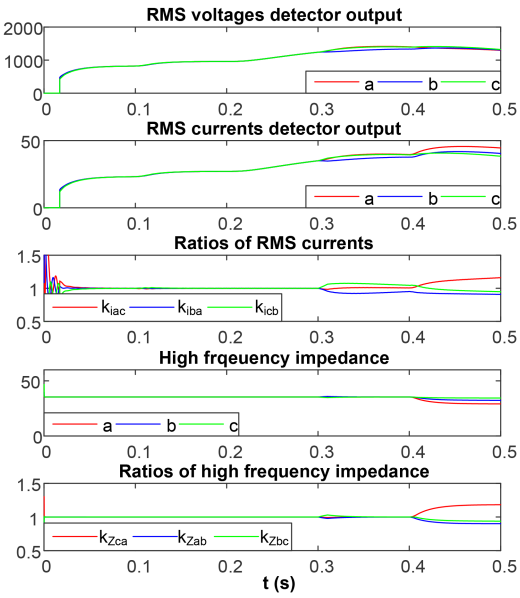

Fig. 7 *Responses of high-frequency currents ratios and high-frequency impedance ratios in transient states*

variation in healthy condition. Thus, a false alarm is unlikely to be triggered by transient states. Also, when faults occur during transient states, they can still be detected and classified successfully, making the detection and classification more reliable and robust.

5 Conclusions

A new detection and classification algorithm for turn fault and HRC fault conditions based on high-frequency impedance and high-frequency PWM ripple current has been described. It has been shown by theoretical analysis that a turn fault gives rise to asymmetric high-frequency impedances in a three-phase SPM machine while three-phase symmetry is maintained under an HRC fault. This difference together with high-frequency PWM ripple currents is used for the fault detection and classification. The utility and effectiveness of the algorithm are demonstrated via the simulations on a three-phase SPM drive.

6 Acknowledgments

This work is sponsored in part by the UK Engineering and Physics Research Council (EPSRC) through PhD studentship and in part by Rolls-Royce plc through Industrial Case Award.

7 References

[1] Zhu, Z.Q., Howe, D.: 'Electrical machines and drives for electric, hybrid, and fuel cell vehicles', *Proc. IEEE*, 2007, **95**, (4), pp. 746–765

[2] Chau, K.T., Chan, C.C., Liu, C.: 'Overview of permanent-magnet brushless drives for electric and hybrid electric vehicles', *IEEE Trans. Ind. Electron.*, 2008, **55**, (6), pp. 2246–2257

[3] Zhang, P., Du, Y., Habetler, T.G., *et al.*: 'A survey of condition monitoring and protection methods for medium-voltage induction motors', *IEEE Trans. Ind. Appl.*, 2011, **47**, (1), pp. 34–46

[4] Grubic, S., Aller, J.M., Lu, B., *et al.*: 'A survey on testing and monitoring methods for stator insulation systems of low-voltage induction machines focusing on turn insulation problems', *IEEE Trans. Ind. Electron.*, 2008, **55**, (12), pp. 4127–4136

[5] Ebrahimi, B.M., Faiz, J., Member, S.: 'Feature extraction for short-circuit fault detection in permanent-magnet synchronous motors using stator-current monitoring', *IEEE Trans. Power Electron.*, 2010, **25**, (10), pp. 2673–2682

[6] Urresty, J.C., Riba, J.R., Romeral, L.: 'Diagnosis of interturn faults in pmsms operating under nonstationary conditions by applying order tracking filtering', *IEEE Trans. Power Electron.*, 2013, **28**, (1), pp. 507–515

[7] Kim, K.-H., Choi, D.-U., Gu, B.-G., *et al.*: 'Online fault-detecting scheme of an inverter-fed permanent magnet synchronous motor under stator winding shorted turn and inverter switch open', *IET Electr. Power Appl.*, 2011, **5**, (6), pp. 529–539

[8] Khan, M., Rahman, M.A.: 'Development and implementation of a novel fault diagnostic and protection technique for IPM motor drives', *IEEE Trans. Ind. Electron.*, 2009, **56**, (1), pp. 85–92

[9] Hang, J., Zhang, J., Cheng, M., *et al.*: 'Online inter-turn fault diagnosis of permanent magnet synchronous machine using zero sequence components', *IEEE Trans. Power Electron.*, 2015, **30**, (12), pp. 6731–6741

[10] Zarri, L., Mengoni, M., Gritli, Y., *et al.*: 'On-line detection of high resistance connections with inverse-sequence regulators in three phase induction motor drives', *IEEE Trans. Ind. Appl*, 2015, **51**, (2), pp. 1579–1586

[11] Mengoni, M., Zarri, L., Tani, A., *et al.*: 'Online detection of high- resistance connections in multiphase induction machines', *IEEE Trans. Power Electron.*, 2015, **30**, (8), pp. 4505–4513

[12] Zhang, J., Hang, J., Ding, S., *et al.*: 'Online diagnosis and localization of high-resistance connection in PMSM with improved fault indicator', *IEEE Trans. Power Electron.*, 2016, **32**, (5), pp. 3585–3594

[13] Yun, J., Cho, J., Bin Lee, S., *et al.*: 'Online detection of high-resistance connections in the incoming electrical circuit for induction motors', *IEEE Trans. Ind. Appl.*, 2009, **45**, (2), pp. 694–702

[14] Yun, J., Lee, K., Lee, K.W., *et al.*: 'Detection and classification of stator turn faults and high-resistance electrical connections for induction machines', *IEEE Trans. Ind. Appl.*, 2009, **45**, (2), pp. 666–675

[15] Sen, B.: 'Modelling, Fault Detection and Control of Fault Tolerant Permanent Magnet Machine Drives'. PhD thesis, Univ. Sheff., September 2015

[16] Sen, B., Wang, J.: 'Analytical modelling of stator turn fault in surface mounted permanent magnet machines'. 2013 IEEE Energy Conversion Congress and Exposition (ECCE 2013), Denver, USA, 2013, pp. 4445–4452

[17] Hu, R., Wang, J., Mills, A.R., *et al.*: 'PWM ripple currents based turn fault detection for 3-phase permanent magnet machines', IEEE Int. Electric Machines Drives Conf., Miami, USA, 2017, pp. 1–7